Impact of temperature dependence on the possible contribution of organics to new particle formation in the atmosphere

Fangqun Yu[1], Gan Luo[1], Alexey B. Nadykto[1, 2], and Jason Herb[1]

[1]Atmospheric Sciences Research Center, State University of New York, 251 Fuller Road, Albany, New York 12203, USA

[2]Department of Applied Mathematics, Moscow State University of Technology "Stankin", Vadkovsky 1, Moscow, Russia

Abstract. Secondary particles formed via new particle formation (NPF) dominate cloud condensation nuclei (CCN) abundance in most parts of the troposphere and are important for aerosol indirect radiative forcing (IRF). Laboratory measurements have shown that certain organic compounds can significantly enhance binary nucleation of sulfuric acid and H_2O. According to our recent study comparing particle size distributions measured in nine forest areas in North America with those predicted by a global size-resolved aerosol model, current H_2SO_4-Organics nucleation parameterizations appear to significantly over-predict NPF and particle number concentrations in summer. The lack of the temperature dependence in the current H_2SO_4-Organics nucleation parameterization has been suggested to be a possible reason for the observed over-prediction. In this work, H_2SO_4-Organics clustering thermodynamics from quantum-chemical studies has been employed to develop a scheme to incorporate temperature dependence into H_2SO_4-Organics nucleation parameterization. We show that temperature has a strong impact on H_2SO_4-Organics nucleation rates, and may reduce nucleation rate by ~ one order of magnitude per 10 K of the temperature increase. The particle number concentrations in summer over North America based on the revised scheme is a factor of more than two lower, in much better agreement with the observations. With the temperature-dependent H_2SO_4-Organics nucleation parameterization, the summer month CCN concentrations in the lower troposphere in the northern hemisphere are about 10-30% lower compared to the temperature independent one. This study highlights the importance of the temperature effect and its impacts on NPF in global modeling of aerosol number abundance.

1. Introduction

Atmospheric particles, through acting as cloud condensation nuclei (CCN), modify cloud properties and precipitation and thus, indirectly, affect the hydrological cycle and climate. Aerosol indirect radiative forcing (IRF) remains a major uncertainty in assessing climate change (IPCC, 2013). Secondary particles formed via nucleation dominate particle number concentrations in many parts of troposphere (Spracklen et al., 2008; Pierce and Adams, 2009; Yu and Luo, 2009), and global simulations indicate that nucleation schemes/parameterizations have a strong effect on the aerosol IRF estimations (Wang and Penner, 2009; Kazil et al., 2010; Yu et al., 2012). Different nucleation schemes, with nucleation rates depending on different variables, predict significantly different spatial patterns and seasonal variations of nucleation rates and CCN concentrations (Yu et al., 2010, 2015). Therefore, it is important to understand mechanisms of new particle formation (NPF) and the key parameters controlling the contribution of the NPF to CCN formation under wide range of varying atmospheric conditions and to validate their representation in regional and global climate models.

A number of laboratory chamber studies indicate that certain organic species can significantly enhance NPF (e.g., Zhang et al., 2004; Riccobono et al., 2014). This finding may have important implications for the interactions of anthropogenic and biogenic emissions and the associated climate forcing. To this regard, it is necessary to assess the ability of organics-enhanced nucleation to explain nucleation phenomena observed in the atmosphere and to determine the contribution of organics to atmospheric NPF and climate implications. In several laboratory studies, empirical parameterization of formation rate as a function of the concentrations of sulfuric acid and low-volatility highly oxidized organics has been derived (Metzger et al., 2010; Riccobono et al., 2014). One of the most important limitations of these

57 empirical parameterizations is that they were derived from the chamber measurements carried

58 out under limited range of well-controlled conditions and, thus, reliably extrapolating these data

59 to a wide range of atmospheric conditions remains a major issue. It should also be noted that

60 empirical activation and kinetic nucleation formulas ($J = k_1[H_2SO_4]$ or $J = k_2[H_2SO_4]^2$) derived

61 from limited field measurements (e.g., Riipinen et al., 2007; Kuang et al., 2008) also do not

62 account for the impact of temperature variations on computed nucleation rates. Although these

63 simple empirical temperature independent nucleation parameterizations have been widely used in

64 global aerosol modeling and aerosol IRF studies (e.g., Spracklen et al., 2008; Wang and Penner,

65 2009; Kazil et al., 2010; Scott et al., 2014; Westervelt et al., 2014; Lupascu et al., 2015), possible

66 impacts of temperature variations were not considered in these studies.

67   In a recent study comparing particle size distributions measured in nine forest areas in North

68 America with those predicted by a global size-resolved (sectional) aerosol model, Yu et al.

69 (2015) showed that H_2SO_4-Organics nucleation parameterization of Riccobono et al. (2014)

70 significantly over-predict NPF and particle number concentrations in summer (Yu et al., 2005).

71 The lack of temperature dependence in the H_2SO_4-Organics nucleation parameterization has

72 been suggested as a possible reason for the observed over-prediction. The main objectives of the

73 present study are (1) to develop a scheme to incorporate temperature dependence into H_2SO_4-

74 Organics nucleation parameterization, (2) to assess the ability of the modified parameterization

75 in explaining the seasonal variations of NPF in NA, and (3) to study the global implications.

76

77 **2.** Methods

78 2.1. Organics-mediated nucleation parameterization with temperature dependence (Nucl-OrgT)

79   Based on the CLOUD chamber study of nucleation process involving sulfuric acid and

80   organic compounds of relatively low volatility from the oxidation of pinanediol, Riccobono et al.

81   (2014) derived the following organics-mediated nucleation parameterization (Nucl-Org),

$$J_{Nucl-Org}=k_m\times[H_2SO_4]^2\times[BioOxOrg] \tag{1}$$

82

83   where $J_{Nucl-Org}$ is the formation rate (# $cm^{-3}s^{-1}$) of particles of ~ 1.7 nm, k_m is the fitting pre-factor

84   with a value of 3.27×10^{-21} cm^6 s^{-1} (90% confidence interval: 1.73×10^{-21} to 6.15×10^{-21} cm^6 s^{-1}),

85     $[H_2SO_4]$ and $[BioOxOrg]$ are the gas-phase concentrations (# cm^{-3}) of H_2SO_4 and biogenic

86   oxidized organic (BioOxOrg) vapors, respectively. In the chamber study reported in Riccobono

87   et al. (2014), BioOxOrg molecules are organic compounds of relatively low volatility from the

88   oxidation of pinanediol (a first-generation oxidation product of α-pinene) and represent later-

89   generation oxidation products of biogenic monoterpenes.

90   The Nucl-Org parameterization given in Eq. 1, derived from laboratory chamber studies at

91   T=278 K and RH=39% (Riccobono et al., 2014), does not consider the possible effect of

92   temperature on nucleation rate. According to the nucleation theory, nucleation rates are

93   temperature-dependent unless nucleation is barrierless and limited by collision rates only.

94   However, the value of the pre-factor k_m of 3.27×10^{-21} cm^6 s^{-1} is well below the three-body

95   collision rate corresponding to the formation of a cluster containing two H_2SO_4 and one

96   BioOxOrg molecules. This indicates that nucleation in the CLOUD chamber under conditions

97   reported in Riccobono et al. (2014) was not barrierless, and, thus, nucleation rates should be

98   temperature-dependent.

99   Based on the classical homogeneous nucleation theory, the rate of nucleation (J) can be

100   generally written in the form

$$J = C_1 \exp(-\Delta G/kT) \tag{2}$$

101

102   where ΔG is the Gibbs free energy needed to form the critical cluster and C_1 is the pre-factor.

103   With $\Delta G = \Delta H - T \Delta S$, where ΔH and ΔS are associated enthalpy and entropy change, we get

104     $$J = C_1 \exp(-\Delta H/kT + \Delta S/k) = C_1 \exp(\Delta S/k) \exp(-\Delta H/kT) = C_2 \exp(-\Delta H/kT) \tag{3}$$

105   The temperature dependence of nucleation rate is dominated by the exponential term in Eq.

106   (3), although C_2 may also weakly depend on temperature. Assuming that C_2 is independent of

107   temperature and using $J_{\text{Nucl-Org}}$ given in Eq. (1) as the nucleation rate at the reference temperature

108     $T_0 = 278$ K, we obtain

109     $$J_{\text{Nucl-OrgT}} = J_{\text{Nucl-Org}} \, f_T \tag{4}$$

110     $$f_T = \exp[\frac{\Delta H}{k} (\frac{1}{T} - \frac{1}{T_0})] \tag{5}$$

111   where f_T is the correction factor accounting for the temperature dependence.

112   One challenge here is to obtain enthalpy change (ΔH) associated with the critical cluster

113   formation because it is quite difficult to determine the chemical identities of BioOxOrg

114   molecules involved in atmospheric nucleation (Elm et al, 2014; Riccobono et al., 2014). As a

115   first order approximation, we use 2-Methyl-5-[(1S,2S,3R)-1,2,3,4-tetrahydroxybutyl]-3-furoic

116   acid, a select highly oxidized organic $C_{10}H_{14}O_7$ compound, as a proxy for BioOxOrg molecules.

117   The stability of the cluster composed of two H_2SO_4 and one $C_{10}H_{14}O_7$ molecules has been

118   investigated using the Density Functional theory (DFT) at PW91PW91/6-311++G(3df,3pd) level.

119   The PW91PW91 is the most common density functional used in atmospheric studies that

120   predicts structure, vibrational spectrums, dipolar properties and thermodynamics of atmospheric

121   molecules and molecular clusters with high degree of confidence and its predictions, which have

122   been systematically validated against experimental and higher level ab initio Gibbs free energies,

123   are in a very good agreement with them for a number of atmospherically relevant molecules and

124 clusters (e.g. Herb et al., 2013, Elm et al., 2013, Nadykto et al., 2015; DePalma et al., 2015).

125 Computations have been carried out using the Gaussian 09 suite of programs (Frish et al., 2009).

126   Figure 1 presents the equilibrium geometry of the most stable isomers of heteromolecular

127 trimer composed of $(C_{10}H_{14}O_7)(H_2SO_4)_2$ and Table 1 reports the corresponding the

128 thermodynamic data associated the formation of this cluster. The computational methodology,

129 benchmarks of Gibbs free energy changes and Cartesian geometries of global minima and local

130 minima located within 1 kcal mol^{-1} of the global minima, along with interactions of $C_{10}H_{14}O_7$

131 and H_2SO_4 with some base molecules, will be detailed in a separate manuscript. Here, as a first

132 order of approximation, we use ΔH value of -38.30 kcal mol^{-1} to calculate the temperature-

133 dependent factor f_T in Eq. (5). Figure 2 shows the calculated value of f_T as a function of T. It is

134 clear from Fig. 2 that f_T decreases significantly as T increases, roughly one order of magnitude

135 per 10 K. When T < 269 K, f_T becomes larger than 10 and increases with decreasing T. f_T is set

136 to have a maximum value so that $J_{Nucl-OrgT}$ does not exceed the 3-body kinetic collision rate for

137 forming a cluster containing two H_2SO_4 molecules and one BioOxOrg molecule, which depends

138 on T as well as the mass and sizes of colliding molecules. At T=270 K, the maximum value of f_T

139 is ~ 38. Compared to the original $J_{Nucl-Org}$ parameterization of Riccobono et al. (2014) (Eq. 1)

140 derived from laboratory chamber studies at T=278 K and not taking into account the temperature

141 dependence of nucleation rates (i.e., f_T =1, dashed line in Fig. 2), the revised parameterization

142 $J_{Nucl-OrgT} = f_T J_{Nucl-Org}$ predicts quite different nucleation rate in the atmosphere, especially in the

143 summer season, when both T and VOC emissions are at peak values.

144   It should be noted that f_T shown in Fig. 2 is subject to large uncertainty because of the

145 potential difference between the molecules involved in the nucleation and the proxy molecule

146 shown in Figure 1. The thermodynamic data for the formation of $(H_2SO_4)_2(BioOxOrg)$ clusters is

147 quite limited. Elm et al. (2014) investigated the molecular interactions between the α-pinene

148 oxidation product pinic acid and sulfuric acid using computational methods and reported a ΔH

149 value of -42.5 kcal/mol for the formation of $(H_2SO_4)_2$(Pinic Acid). More negative ΔH implies

150 stronger temperature dependence. The sensitivity of f_T values to ΔH can be readily calculated

151 from Eq. (4). For example, a fairly large uncertainty of 5 kcal mol^{-1} in ΔH leads to the

152 uncertainty in f_T of a factor of ~ 1.4 at T=288 K, while the extremely large 20 kcal mol^{-1}

153 variation in ΔH alters f_T at T=288 K by a factor of ~ 3.5. The sensitivity of predicted nucleation

154 rates and particle number concentrations to ΔH values is presented in Section 3. Despite possible

155 uncertainties in f_T, the temperature dependent $J_{Nucl-OrgT}$ is likely to be more realistic than $J_{Nucl-Org}$,

156 in which the temperature dependence is neglected.

157

158 2.2. GEOS-Chem model and global simulations

159 This work represents a major global modeling attempt in studying the effect of temperature

160 on organics-mediated nucleation in the atmosphere. This study is built upon the work reported in

161 Yu et al. (2015) and, thus, we use the same global model (GEOS-Chem) and configurations as

162 that described in Yu et al. (2015). GEOS-Chem is a global 3-D model of atmospheric

163 composition driven by assimilated meteorological observations from the Goddard Earth

164 Observing System (GEOS) of the NASA Global Modeling and Assimilation Office (GMAO)

165 (e.g., Bey et al., 2001). More detailed information about GEOS-Chem and updates can be found

166 at the model website (http://geos-chem.org/). The aerosol simulation is based on a size-resolved

167 (sectional) advanced particle microphysics (APM) model incorporated into GESO-Chem by Yu

168 and Luo (2009) and considers the successive oxidation aging of the oxidation products of various

169 VOCs (Yu, 2011). In GEOS-Chem v8-03-02, on which this study and previous work (Yu et al.,

170 2015) are based, the concentration of highly oxidized low volatile secondary organic gas from

171 the oxidation products of α-pinenes (LV-SOG$_{\alpha\text{-pinene}}$) is explicitly simulated and used in Eqs. (1)

172 and (4) to calculate organics-mediated nucleation rates. The horizontal resolution of GEOS-

173 Chem employed in this study is $2^o \times 2.5^o$ and there are 47 vertical model layers (with 14 layers

174 from surface to ~ 2 km above the surface). Other relevant model configurations (including

175 emission inventories and various schemes) can be found in Yu et al. (2015).

176   The main difference between the present study and the previous one reported by Yu et al.

177 (2015) is that the present study employs the T-dependent Nucl-Org parameterization given in Eq.

178 (4) instead of T-independent parameterization of Riccobono et al. (2014). In addition, study of

179 Yu et al. (2015) focuses only on the NA region, while in this work, the discussion on organics-

180 mediated nucleation is expanded to the whole globe.

181

182 **3. Results**

183   Figure 3 shows the effect of T-dependent correction factor on simulated global distributions

184 of monthly mean (July, 2006) nucleation rates, particle number and CCN concentrations in the

185 boundary layer (0-1 km above the surface). The high biogenic VOC emissions in the summer

186 coupled with strong photochemistry lead to higher concentrations of LV-SOG$_{\alpha\text{-pinene}}$ or

187 BioOxOrg (Yu et al., 2015) and hence, according to the parameterization of Riccobono et al.

188 (2014) (i.e., Eq. 1), significant organics-mediated nucleation (Fig. 3a) and higher particle number

189 concentrations (Figs. 3c and 3e). However, the high temperature in the summer substantially

190 lower nucleation rates (Fig. 3b), and reduce the global monthly mean nucleation rate in the

191 boundary layer from 0.17 $cm^{-3}s^{-1}$ (Fig. 3a) to 0.02 $cm^{-3}s^{-1}$, with stronger effect in the northern

192   hemisphere (Fig. 3b). As a result, the global monthly mean CN10 and CCN0.4 in the boundary

193   layer decrease by 40% and 30%, respectively.

194   A ΔH value of -38.3 kcal mol^{-1} was used in calculating $J_{Nucl-OrgT}$ in Fig. 3b. The impact of ΔH

195   values (from 0 to 58.3 kcal mol^{-1}) on $J_{Nucl-OrgT}$, CN10 and CCN0.4 averaged in the boundary

196   layer over the whole globe for the same summer month is presented in Figure 4. A zero value of

197   ΔH corresponds to the case of no T-dependent correction (i.e., $J_{Nucl-Org}$, Fig. 3a). $J_{Nucl-OrgT}$, CN10

198   and CCN0.4 are more sensitive to ΔH when ΔH is small ($<\sim$ 30 kcal mol^{-1}), with $J_{Nucl-OrgT}$

199   decreasing by a factor of 5, CN10 by 33% and CCN0.4 by 28% as ΔH increases from 0 to 28.3

200   kcal mol^{-1}. Further increase of ΔH from 28.3 to 58.3 kcal mol^{-1} reduces $J_{Nucl-OrgT}$, CN10 and

201   CCN0.4 by 100%, 25%, and 10%, respectively. It can be seen from Figure 4 that the T-

202   dependent correction, even with a smaller value of ΔH, is important. On the other hand, the

203   effect of potential uncertainty in ΔH around the values derived from quantum calculation ($\sim$ 40

204   kcal mol^{-1}, see Section 2.1) is relatively weaker.

205   As we have pointed out earlier, the previous comparisons of simulated and observed particle

206   size distributions measured in nine forest areas in North America (NA) (Yu et al., 2005) showed

207   that $J_{Nucl-Org}$ parameterization (Eq. 1) over-predicts condensation nuclei number concentrations in

208   the size range of 10 and 100 nm (CN_{10-100}) at these sites in summer by a factor of around two on

209   average (Yu et al., 2005). To examine the extent, at which the revised parameterization

210   considering T-dependence (Eq. 4) can improve the agreement of simulations with measurements,

211   we present the monthly mean horizontal distributions of CN10 zoomed into the NA region in Fig.

212   5 and observed and simulated CN_{10-100} averaged over the nine forest sites in Fig. 6. It can be

213   clearly seen from Fig. 5 that the simulated monthly mean CN10 values in the NA boundary layer

214   based on $J_{Nucl-OrgT}$ (Eq. 4) are about a factor of two lower than those based on $J_{Nucl-Org}$ (Eq. 1),

215 with larger difference in the lower latitude part of the domain, where T is higher. In the case,

216 when the effect of T on Nucl-Org is taken into account, the domain-wide average CN10 value

217 decreases from 4600 to 2200 $\#/cm^3$ and Figure 6 shows that the simulated CN_{10-100} averaged over

218 the nine forest sites (with locations marked on Fig. 5, see Yu et al. (2015) for details) agrees

219 much better with that of observed. It can also be seem from Fig. 6 that CN_{10-100} over the NA

220 forest sites is more sensitive to ΔH values than the global mean CN10 shown in Fig. 4, and ΔH

221 of ~35 kcal mol^{-1} agrees best with the observations.

222   To further illustrate the difference and improvement for the cases with and without T-

223 dependent correction, we present in Fig. 7 a set of detailed comparisons of simulated and

224 observed evolution of particle size distributions during two ten-day periods in March and July of

225 2006 in Duke Forest (Pillai et al., 2013), along with time series of CN_{10-100} (integrated from

226 PSDs), which give a good overall representation of particle nucleation and growth. The observed

227 PSDs and simulated PSDs based on $J_{Nucl-Org}$ has been discussed in Yu et al. (2015) and are

228 repeated here for comparison with $J_{Nucl-OrgT}$ scheme in order to demonstrate the impact of

229 temperature on nucleation and particle number concentrations. Although the present work

230 focuses on the summer month, when the largest difference between $J_{Nucl-Org}$ prediction and

231 observation is observed, we also show in Fig. 7 simulations for a 10-day period in March as well

232 for the comparison purpose. NPF events observed in Duke Forest are much more frequent and

233 concentrations of nucleation mode particles are much higher in the spring than in the summer

234 (Figs. 7a & 7b). The temperature correction (Eq. 4) has small effect in the spring (Figs. 7c, 7e,

235 and 7g) but significantly reduces nucleation rate and particle number concentration in summer

236 (Figs. 7d, 7e, and 7f). $J_{Nucl-Org}$ scheme (Eq. 1) predicts strong nucleation events (Fig. 7d) and

237 significant diurnal variations in CN_{10-100} (Fig. 7h) almost every day in the summer period that

238 obviously contradicts to observations (Fig. 7b). The high nucleation rates in the summer based

239 on $J_{Nucl-Org}$ scheme can be easily explained by the much higher BioOxOrg concentrations as a

240 result of high VOC emissions and stronger photochemistry. Nevertheless, the high T in the

241 summer inhibits nucleation (Eq. 4) and the temperature correction factor substantially improves

242 the agreement of the simulated evolution of PSDs (Figs. 7b, 7d, 7f) and CN_{10-100} (Fig. 7h) with

243 observations.

244 Figure 8 shows the ratios of the CCN concentration in the lower troposphere (0-3 km) based

245 on Nucl-Org to the CCN concentration based on Nucl-OrgT. The CCN concentrations are

246 calculated at a water supersaturation ratio of 0.2% (CCN0.2) from simulated PSDs. As a result of

247 higher nucleation rates, CCN0.2 based on Nucl-Org are about 10-20% higher than those based

248 on Nucl-OrgT in July over most parts of northern hemisphere (Fig. 6a), with the largest

249 difference up to 30-70% reached over part of NA, Europe, and Asia.

250 **4. Summary and discussion**

251 Simple empirical nucleation parameterizations, which were derived from laboratory or field

252 measurements under limited conditions and do not consider any temperature dependence of

253 nucleation rates, have been widely used in global aerosol modeling and aerosol indirect radiative

254 forcing studies. Based on the classical nucleation theory, temperature should be one of key

255 parameters controlling nucleation rates, unless nucleation is barrierless. A recent study indicates

256 (Yu et al., 2015) that the empirical parameterization of H_2SO_4-Organics nucleation of Riccobono

257 et al. (2014) significantly over-predicts NPF and particle number concentrations in North

258 America in summer. The lack of temperature dependence in the parameterization has been

259 suggested as a likely reason for the observed over-prediction. In the present study, H_2SO_4-

260 Organics clustering thermodynamics from quantum-chemical studies has been employed to

261 develop a scheme for incorporating the temperature dependence into H_2SO_4-Organics nucleation

262 parameterization, which reduces global mean nucleation rate in the boundary layer in a summer

263 month is by a factor of ~ 8 and improves the agreement of predicted particle number

264 concentrations over North America with observations. With temperature-dependent H_2SO_4-

265 Organics nucleation parameterization, the summer month CCN concentrations in the lower

266 troposphere in the northern hemisphere are about 10-30% lower. In view of the potential effects

267 of changes in CCN concentrations on precipitation (second indirect impact) and cloud cover, it is

268 important to reduce uncertainties in NPF calculation in regional and global climate models.

269   The study highlights the importance of including the temperature dependence of nucleation

270 rates in global modeling of NPF and aerosol indirect radiative forcing. In a recent study, Dunne

271 et al. (2016) also showed a substantial impact of the temperature dependence on the contribution

272 of organic nucleation to overall nucleation. The temperature dependence factor derived under

273 this study can be applied to study the temperature effect on organics-mediated nucleation in the

274 global atmosphere and improve the agreement of simulated particle number concentrations with

275 observations. Although it may subject to uncertainties due to the possible difference between the

276 molecules involved in the nucleation and the proxy molecule, temperature dependent $J_{Nucl-OrgT}$,

277 likely more realistic than $J_{Nucl-Org}$, in which the temperature dependence is neglected. Further

278 laboratory measurements and theoretical studies are needed to better understand the effect of

279 temperature on organics-mediated nucleation in the atmosphere.

280

281 **Acknowledgments**. This study was supported by NASA under grant NNX13AK20G and the

282 National Science Foundation (NSF) under grant 1550816. We would like to acknowledge high-

283 performance computing support from Yellowstone (ark:/85065/d7wd3xhc) provided by NCAR's

284 Computational and Information Systems Laboratory, sponsored by the NSF. The GEOS-Chem

285 model is managed by the Atmospheric Chemistry Modeling Group at Harvard University with

286 support from NASA's Atmospheric Chemistry Modeling and Analysis Program.

287

288 **References**

289 Bey, I., Jacob, D. J. Yantosca, R. M. , Logan, J. A. Field, B. Fiore, A. M. Li, Q., Liu, H.,

290   Mickley, L. J., and Schultz, M.: Global modeling of tropospheric chemistry with assimilated

291   meteorology: Model description and evaluation, Journal of Geophysical Research, 106,

292   23,073–23,096, 2001.

293 DePalma, J. W., J. Wang, A. S. Wexler, and M.V Johnston, Growth of ammonium bisulfate

294   clusters by adsorption of oxygenated organic molecules, The Journal of Physical Chemistry

295   A, 119 (45), 11191–11198, DOI: 10.1021/acs.jpca.5b07744, 2015.

296 Dune et al., Global atmospheric particle formation from CERN CLOUD measurements, Science,

297   354, 6316, DOI:10.1126/science.aaf2649, 2016.

298 Elm, J., M. Bilde, and K. V. Mikkelsen: Assessment of binding energies of atmospherically

299   relevant clusters. Physical Chemistry Chemical Physics 15.39, 16442-16445., 2013.

300 Elm, J., T. Kurten, M. Bilde and K.V. Mikkelsen: Molecular interaction of pinic acid with

301   sulfuric acid: Exploring the thermodynamic landscape of cluster growth, The Journal of

302   Physical Chemistry A, 2014, 118, 7892−7900, 2014.

303 Frisch, M. J.; Trucks, G. W.; Schlegel, H. B.; Scuseria, G. E.; Robb, M. A.; Cheeseman, J. R.;

304   Scalmani, G.; Barone, V.; Mennucci, B.; et al.: Gaussian 09, Gaussian, Inc., Wallingford CT,

305   2009.

Herb, J., Y. Xu, F. Yu, and A. B. Nadykto, Large hydrogen-bonded pre-nucleation (HSO_4^-) (H_2SO_4)$_m$(H_2O)$_k$ and (HSO_4^-)(NH_3)(H_2SO_4)$_m$(H_2O)$_k$ Clusters in the Earth's Atmosphere, The Journal of Physical Chemistry A, *117* (1), 133–152, 2013.

IPCC, Climate Change 2013: The Physical Scientific Basis, edited by T. F. Stocker, D. Qin, et al., Cambridge Univ. Press, New York, USA, 2013.

Kazil, J., Stier, P., Zhang, K., Quaas, J., Kinne, S., O'Donnell, D., Rast, S., Esch, M., Ferrachat, S., Lohmann, U., and Feichter, J.: Aerosol nucleation and its role for clouds and Earth's radiative forcing in the aerosol-climate model ECHAM5-HAM, Atmospheric Chemistry and Physics, 10, 10733-10752, doi:10.5194/acp-10-10733-2010, 2010.

Kuang, C., McMurry, P. H., McCormick, A. V., and Eisele, F. L.: Dependence of nucleation rates on sulfuric acid vapor concentration in diverse atmospheric locations, J. Geophys. Res., 113, D10209, doi:10.1029/2007JD009253, 2008.

Lupascu, A., Easter, R., Zaveri, R., Shrivastava, M., Pekour, M., Tomlinson, J., Yang, Q., Matsui, H., Hodzic, A., Zhang, Q., and Fast, J. D.: Modeling particle nucleation and growth over northern California during the 2010 CARES campaign, Atmos. Chem. Phys., 15, 12283-12313, doi:10.5194/acp-15-12283-2015, 2015.

Metzger, A., Verheggen, B., Dommen, J., Duplissy, J., Prevot, A.S., Weingartner, E., Riipinen, I., Kulmala, M., Spracklen, D.V., Carslaw, K.S. and Baltensperger, U.: Evidence for the role of organics in aerosol particle formation under atmospheric conditions, Proceedings of the National Academy of Sciences, 107(15), pp.6646-6651, 2010.

Nadykto, A. B., J. Herb, F.Yu, and Y. Xu: Enhancement in the production of nucleating clusters due to dimethylamine and large uncertainties in the thermochemistry of amine-enhanced nucleation, Chemical Physics Letters, 609, 42-49, 2015.

329 Pierce, J.R., and Adams, P.J.: Uncertainty in global CCN concentrations from uncertain aerosol

330   nucleation and primary emission rates, Atmospheric Chemistry and Physics, 9, 1339-1356,

331   2009.

332 Pillai, P., Khlystov, A., Walker, J. and Aneja, V. Observation and analysis of particle nucleation

333   at a forest site in southeastern US. Atmosphere. 4(2):72-93, 2013.

334 Riccobono, FSchoberberger, S., Scott, C.E., Dommen, J., Ortega, I.K., Rondo, L., Almeida, J.,

335   Amorim, A., Bianchi, F., Breitenlechner, M., David, A., Downard, A., Dunne, E.M.,

336   Duplissy, J., Ehrhardt, S., Flagan, R.C., Franchin, A., Hansel, A., Juuninen, H., Kajos, M.,

337   Keskinen, H., Kupc, A., Kürten, A., Kvashin, A.N., Laaksonen, A., Lehtipalo, K.,

338   Makkmutov, V., Mathot, S., Nieminen, T., Onnela, A., Petäjä, T.,Praplan, A.P., Santos, F.D.,

339   Schallhart, S., Seinfeld, J.H., Sipilä, M., Spracklen, D.V., Stozhkov, Y., Stratmann, F., Tomé,

340   A., Tsagkogeorgas, G., Vaattlovaara, P., Viisanen, Y., Vrtala, A., Wagner, P.E., Weingartner,

341   E., Wex, H., Wimmer, D., Carslaw, K.S., Curtius, J., Donahue, N.M., Kirkby, J., Kulmala, M.

342   Worsnop, D.R., and Baltensperger, U.: Oxidation products of biogenic emissions contribute

343   to nucleation of atmospheric particles, Science, 344, 717, 2014.

344 Riipinen, I., S.-L. Sihto, M. Kulmala, F. Arnold, M. Dal Maso, W. Birmili, K. Saarnio, K.

345   Teinilä, V.-M. Kerminen, A. Laaksonen, and K. E. J. Lehtinen: Connections between

346   atmospheric sulphuric acid and new particle formation during QUEST III–IV campaigns in

347   Heidelberg and Hyytiälä, Atmos. Chem. Phys., 7, 1899-1914, 2007.

348 Scott, C. E., Rap, A., Spracklen, D. V., Forster, P. M., Carslaw, K. S., Mann, G. W., Pringle, K.

349   J., Kivekäs, N., Kulmala, M., Lihavainen, H., and Tunved, P.: The direct and indirect

350   radiative effects of biogenic secondary organic aerosol, Atmos. Chem. Phys., 14, 447-470,

351   doi:10.5194/acp-14-447-2014, 2014.

352 Spracklen, D. V., Carslaw, K. S., Kulmala, M., Kerminen, V.-M.,Sihto, Riipinen, I., Merikanto,

353 J., Mann, G.W., Chipperfield, M.P., Wiedensohler, A., Birmili, W., and Lihavainen, H.:

354 Contribution of particle formation to global cloud condensation nuclei concentrations,

355 Geophysical Research Letters, 35, L06808, doi:10.1029/2007GL033038, 2008.

356 Wang, M. and Penner, J. E.: Aerosol indirect forcing in a global model with particle nucleation,

357 Atmospheric Chemistry and Physics, 9, 239–260, 2009.

358 Westervelt, D. M., Pierce, J. R., and Adams, P. J.: Analysis of feedbacks between nucleation rate,

359 survival probability and cloud condensation nuclei formation, Atmos. Chem. Phys., 14,

360 5577-5597, doi:10.5194/acp-14-5577-2014, 2014.

361 Yu, F.: A secondary organic aerosol formation model considering successive oxidation aging and

362 kinetic condensation of organic compounds: global scale implications, Atmospheric

363 Chemistry and Physics, 11, 1083-1099, doi:10.5194/acp-11-1083-2011, 2011.

364 Yu, F., and G. Luo: Simulation of particle size distribution with a global aerosol model:

365 contribution of nucleation to aerosol and CCN number concentrations. Atmospheric

366 Chemistry and Physics, 9, 7691-7710, 2009.

367 Yu, F., G. Luo , T. Bates , B. Anderson , A. Clarke , V. Kapustin , R. Yantosca , Y. Wang , S.

368 Wu: Spatial distributions of particle number concentrations in the global troposphere:

369 Simulations, observations, and implications for nucleation mechanisms, J. Geophys. Res.,

370 115, D17205, doi:10.1029/2009JD013473, 2010.

371 Yu, F., Luo, G., Liu, X., Easter, R. C., Ma, X., and Ghan, S. J.: Indirect radiative forcing by ion-

372 mediated nucleation of aerosol, Atmospheric Chemistry and Physics, 12, 11451-11463, 2012.

373   Yu, F., X. Ma, and G. Luo: Anthropogenic contribution to cloud condensation nuclei and the

374   first aerosol indirect climate effect, Environmental Research Letters 8 024029

375   doi:10.1088/1748-9326/8/2/024029, 2013.

376   Yu, F., Luo, G., Pryor, S. C., Pillai, P. R., Lee, S. H., Ortega, J., Schwab, J. J., Hallar, A. G.,

377   Leaitch, W. R., Aneja, V. P., Smith, J. N., Walker, J. T., Hogrefe, O., and Demerjian, K. L.:

378   Spring and summer contrast in new particle formation over nine forest areas in North

379   America, Atmos. Chem. Phys., 15, 13993-14003, doi:10.5194/acp-15-13993-2015, 2015.

380   Zhang, R., I. Suh, J. Zhao, D. Zhang, E.C. Fortner, X. Tie, L.T. Molina, and M.J. Molina:

381   Atmospheric new particle formation enhanced by organic acids, Science, 304, 1487-1490,

382   2004.

383

384

385

386   Table 1. Changes of enthalpy (ΔH), entropy (ΔS), and Gibbs free energy (ΔG) for the formation

387   of $(C_{10}H_{14}O_7)$ $(H_2SO_4)_2$ cluster under the standard condition (P= 1 atm, T=298 K).

	ΔH (kcal mol^{-1})	ΔS (cal mol^{-1}K^{-1})	ΔG (kcal mol^{-1})
$C_{10}H_{14}O_7 + H_2SO_4 + H_2SO_4 \leftrightarrows$ $(C_{10}H_{14}O_7)(H_2SO_4)_2$	-38.30	-75.45	-15.81

388

389 **Figure Captions**

390 **Figure 1**. Equilibrium geometry of the most stable isomers of heteromolecular trimer composed

391 of $(C_{10}H_{14}O_7)$ $(H_2SO_4)_2$ obtained at PW91PW91/6-311++G(3df,3pd) level of theory. Bonding

392 lengths are in angstroms.

393 **Figure 2**. Calculated temperature dependence correction factor for Nucl-Org parameterization

394 (f_T) as a function of T.

395 **Figure 3**. Horizontal distributions of monthly mean nucleation rates (J) (a, b), concentrations of

396 condensation nuclei larger than 10 nm (CN10) (c, d), and concentrations of cloud condensation

397 nuclei at water supsaturation ratio of 0.4% (CCN0.4) (e, f) in the boundary layer (0-1 km above

398 the surface) in July of 2006 based on two organics-mediated nucleation schemes: $J_{Nucl-Org}$ (left

399 panels) and $J_{Nucl-OrgT}$ (right panels).

400 **Figure 4.** Dependence of organics-mediated nucleation rates (left axis), CN10 and CCN0.4

401 (right-axis) averaged in the boundary layer (0-1 km) over the whole globe for July 2006 on ΔH

402 values assumed in calculating temperature dependence correction factor for Nucl-Org

403 parameterization (f_T).

404 **Figure 5.** Horizontal distributions of monthly mean CN10 in the boundary layer (0-1 km above

405 surface) in July of 2006 based on two organics-mediated nucleation schemes: (a) $J_{Nucl-Org}$ and (b)

406 $J_{Nucl-OrgT}$. The locations of 9 forest sites where observed particle size distributions measurements

407 have been used for comparisons in Yu et al. (2015) are marked.

408 **Figure 6.** Effect of ΔH values on simulated number concentrations of condensation nuclei in the

409 size range of 10 and 100 nm (CN_{10-100}) in the boundary layer (0-1 km) for July 2006 averaged

410 over nine forest sites in North America (NA) (locations marked on Fig. 5). The horizontal dashed

411 line shows the average of CN_{10-100} observed in a summer month at the 9 sites.

412   **Figure 7.** Particle size distributions (PSDs) observed (a, b) and simulated based on Nucl-Org (c,

413   d) and Nucl-OrgT (e, f) schemes during two ten-day periods in March (a, c, e) and July (b, d, f)

414   of 2006 in Duke Forest (DUK), along with time series of the concentration of condensation

415   nuclei between 10 and 100 nm ($CN_{10\text{-}100}$) (g, h).

416   **Figure 8.** Ratios of the concentration of CCN (at water supersaturation ratio of 0.2%) in the

417   lower troposphere (0-3 km) based on Nucl-Org scheme to those based on Nucl-OrgT scheme.

418

419
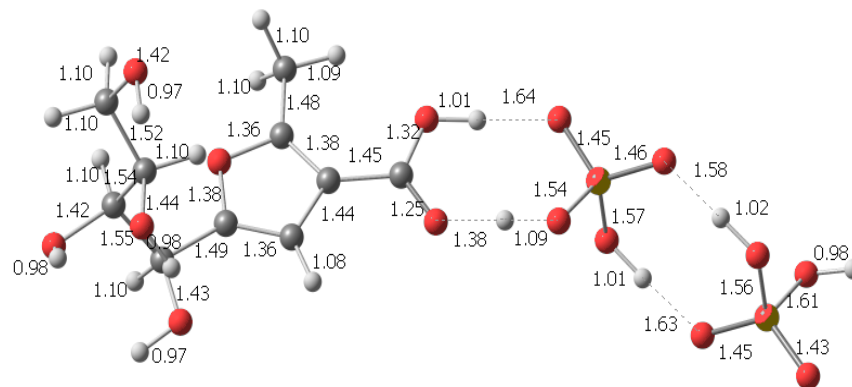
420

421   Figure 1.

422

423
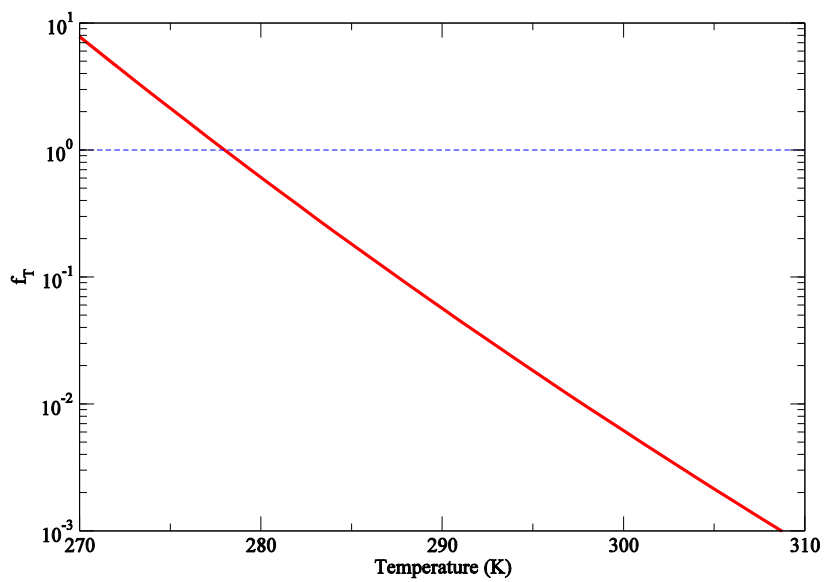
424
425
426   Figure 2.
427

428
429
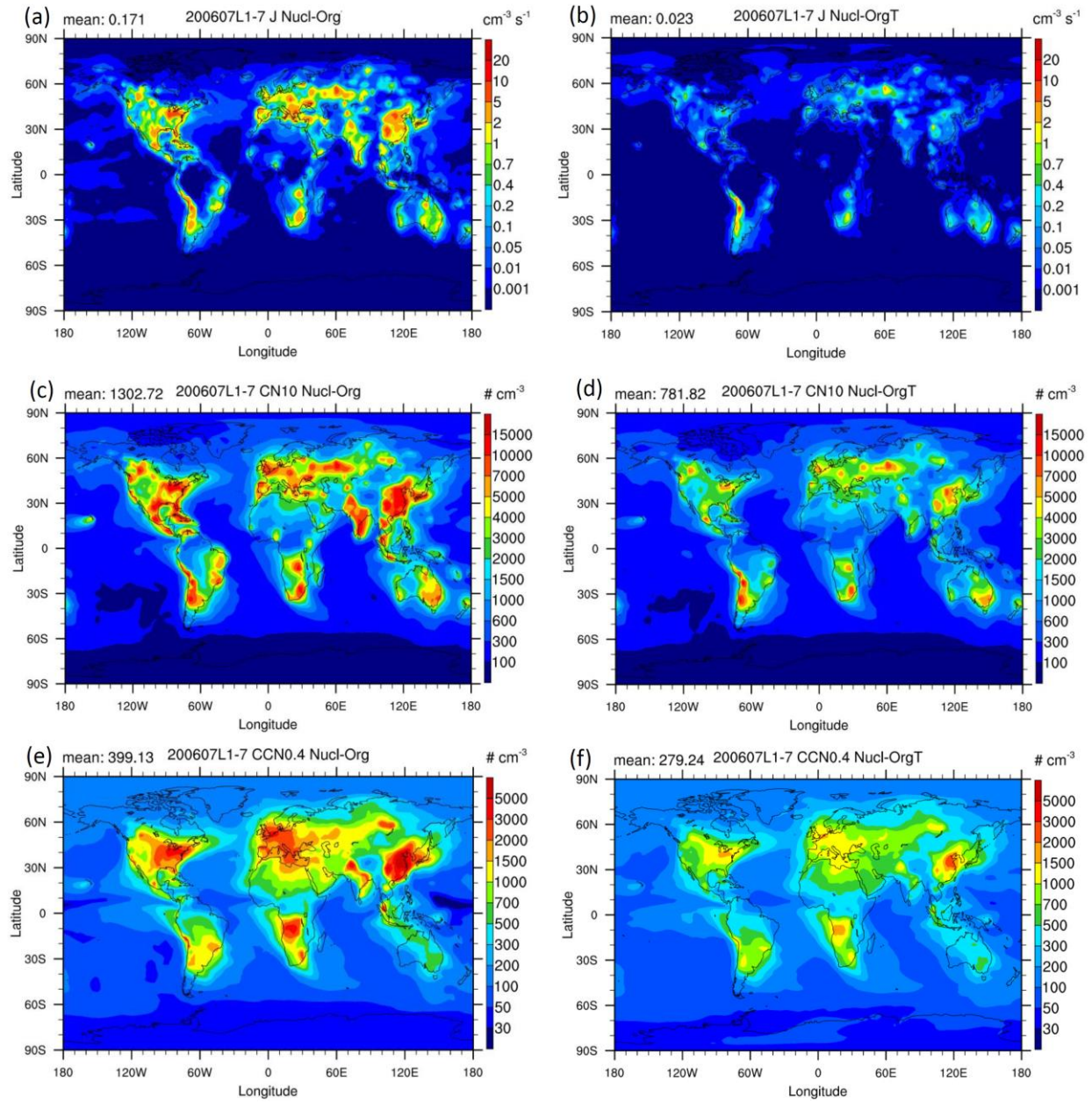
430
431   Figure 3.
432
433
434
435
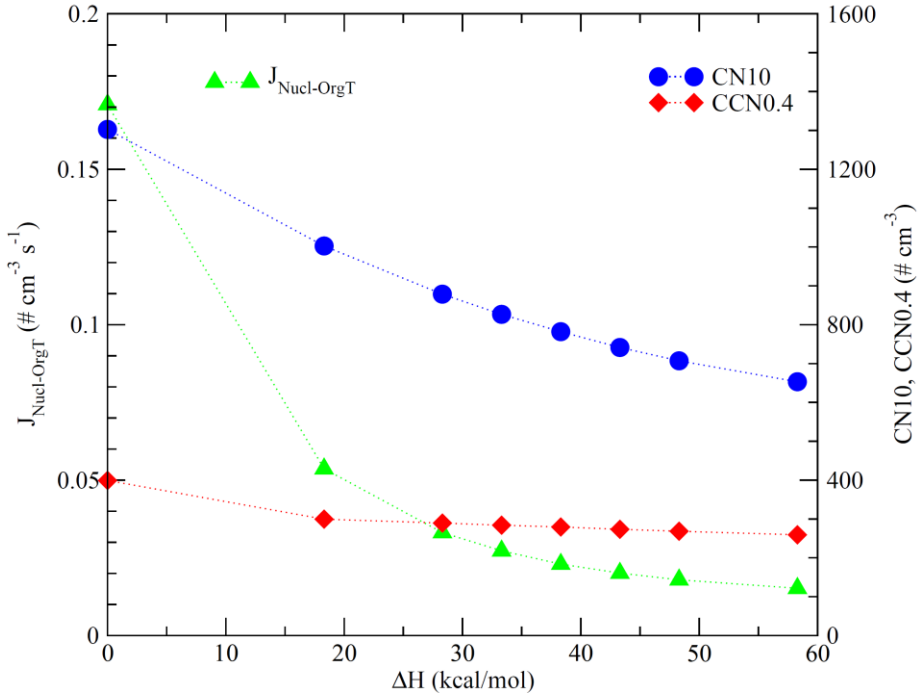
436
437
438   Figure 4.
439
440
441
442
443
444

445
446   Figure 5.

447

448
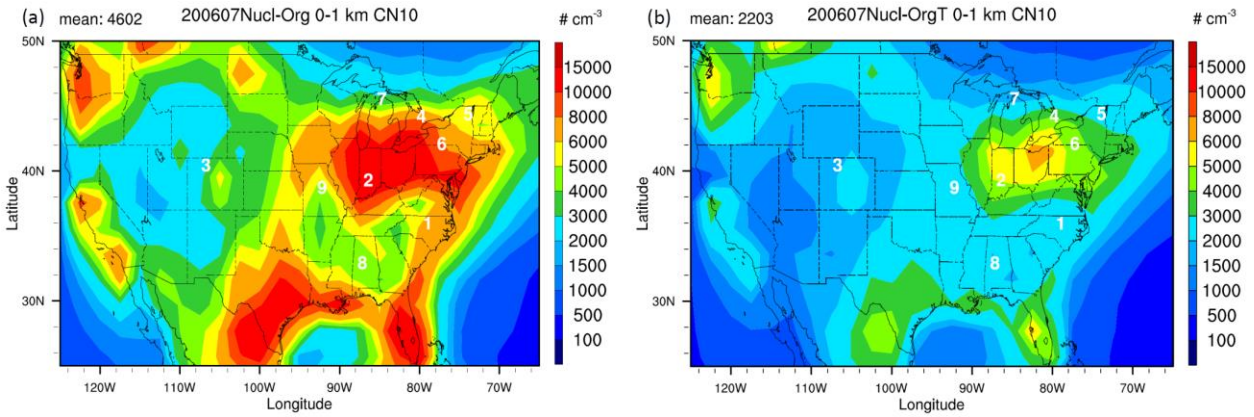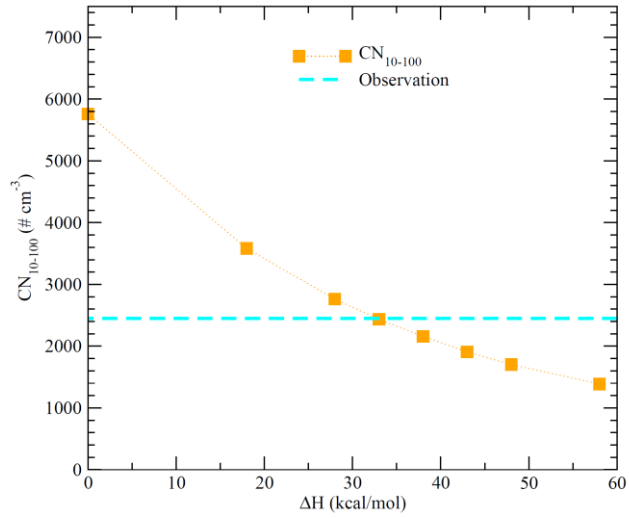
449

450   Figure 6.

451

452
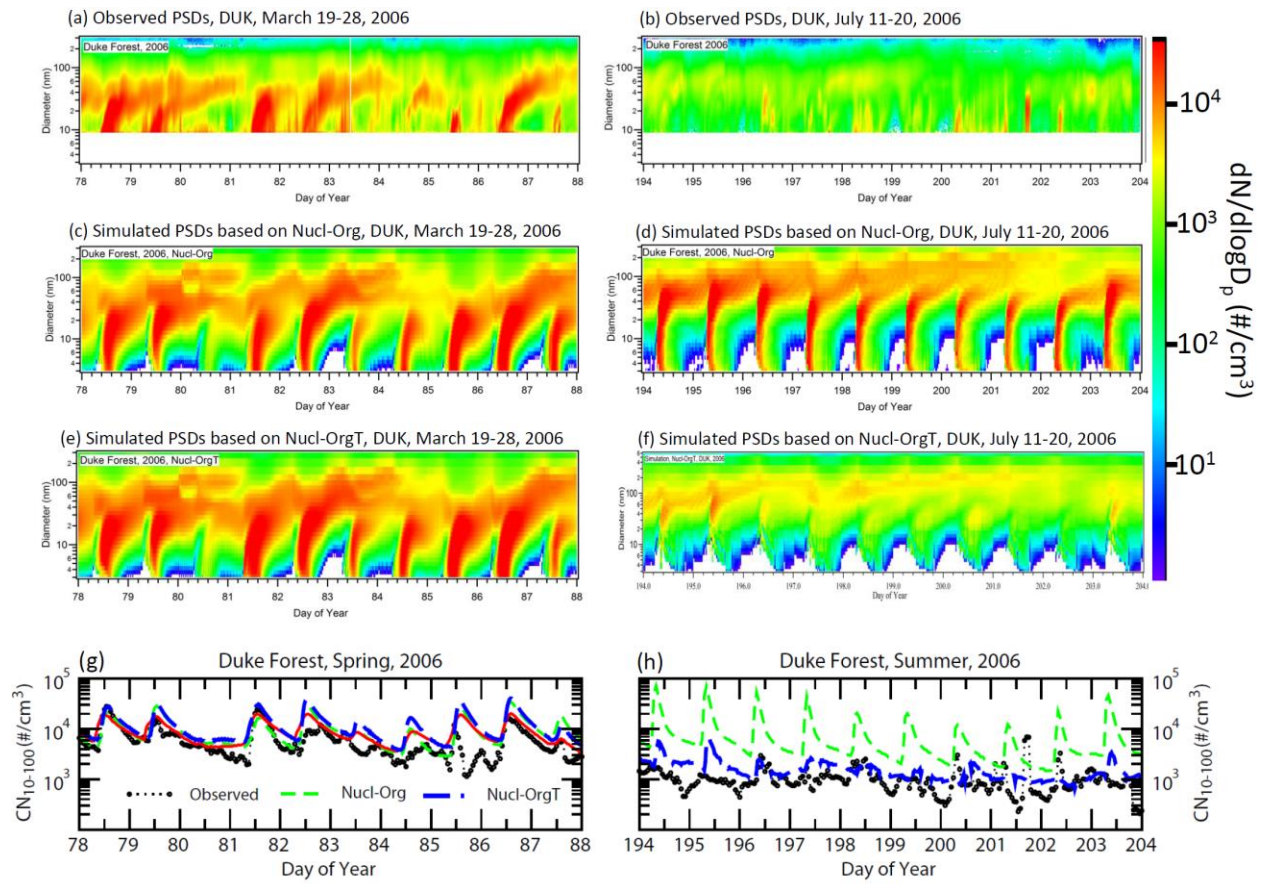
453

454   Figure 7.

455

456

457

458   Figure 8.

459